

Search for B_c^+ decays to two charm mesons

LHCb Collaboration

Received 14 December 2017; received in revised form 2 March 2018; accepted 30 March 2018

Editor: Hong-Jian He

Abstract

A search for decays of B_c^+ mesons to two charm mesons is performed for the first time using data corresponding to an integrated luminosity of 3.0 fb^{-1} , collected by the LHCb experiment in pp collisions at centre-of-mass energies of 7 and 8 TeV. The decays considered are $B_c^+ \rightarrow D_{(s)}^{(*)+} \bar{D}^{(*)0}$ and $B_c^+ \rightarrow D_{(s)}^{(*)+} D^{(*)0}$, which are normalised to high-yield $B^+ \rightarrow D_{(s)}^+ \bar{D}^0$ decays. No evidence for a signal is found and limits are set on twelve B_c^+ decay modes.

© 2018 The Author(s). Published by Elsevier B.V. This is an open access article under the CC BY license (<http://creativecommons.org/licenses/by/4.0/>). Funded by SCOAP³.

1. Introduction

Flavour transitions between quarks are governed in the Standard Model (SM) of elementary particle physics by the Cabibbo–Kobayashi–Maskawa (CKM) quark-mixing matrix [1,2]. Here the transition amplitudes between up-type quarks, q , and down-type quarks, q' , are described by the complex numbers $V_{qq'}$, defining the 3×3 unitary CKM matrix. Precision measurements of the magnitude and phase of the CKM matrix elements may reveal signs of new physics if observables that could be affected by new particles are found to be inconsistent with SM predictions.

One parameter of particular interest is $\gamma \equiv \arg(-V_{ud}V_{ub}^*/V_{cd}V_{cb}^*)$, which can be determined experimentally with negligible theoretical uncertainties from the charge-parity (CP) asymmetry caused by the interference between $b \rightarrow u$ and $b \rightarrow c$ transitions. Presently, the most precise determinations of γ come from measurements of the CP asymmetry in $B^+ \rightarrow \bar{D}^0 K^+$ decays [3,4].¹

¹ Unless specified otherwise, charge conjugation is implied throughout the paper.

Table 1

Estimates of the branching fractions of four $B_c^+ \rightarrow D_{(s)}^+ \bar{D}^0$ decays in units of 10^{-6} . Decays of the B_c^+ meson to final states with one or two excited charm mesons have similar branching fractions and can be found in the cited references.

Channel	Prediction for the branching fraction [10^{-6}]			
	Ref. [9]	Ref. [10]	Ref. [11]	Ref. [12]
$B_c^+ \rightarrow D_s^+ \bar{D}^0$	2.3 ± 0.5	4.8	1.7	2.1
$B_c^+ \rightarrow D_s^+ D^0$	3.0 ± 0.5	6.6	2.5	7.4
$B_c^+ \rightarrow D^+ \bar{D}^0$	32 ± 7	53	32	33
$B_c^+ \rightarrow D^+ D^0$	0.10 ± 0.02	0.32	0.11	0.32

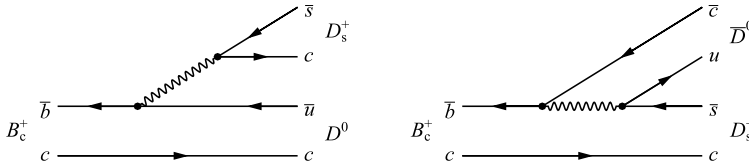


Fig. 1. Illustration of (left) a colour-favoured $B_c^+ \rightarrow D_s^+ D^0$ decay, and (right) a colour-suppressed $B_c^+ \rightarrow D_s^+ \bar{D}^0$ decay.

Decays of B_c^+ mesons to two charm mesons, $B_c^+ \rightarrow D_{(s)}^+ \bar{D}^0$, have also been proposed to measure γ [5–8]. Decays with one excited charm meson in the final state, $B_c^+ \rightarrow D_{(s)}^{*+} \bar{D}^0$ and $B_c^+ \rightarrow D_{(s)}^+ \bar{D}^{*0}$, can be used for measuring the angle γ in the same way as $B_c^+ \rightarrow D_{(s)}^+ \bar{D}^0$ decays. For B_c^+ decays with two excited charm mesons, $B_c^+ \rightarrow D_{(s)}^{*+} \bar{D}^{*0}$, angular distributions provide an alternative method to determine γ [7]. Some predicted branching fractions are listed in Table 1.

In the determination of γ , an advantage of $B_c^+ \rightarrow D_s^+ \bar{D}^0$ decays over $B^+ \rightarrow \bar{D}^0 K^+$ decays is that the diagram proportional to V_{cb} is colour suppressed, while the diagram proportional to V_{ub} is not, as illustrated in Fig. 1. This results in a large value for the ratio of amplitudes, $r_{B_c^+} \equiv |A(B_c^+ \rightarrow D^0 D_s^+)/A(B_c^+ \rightarrow \bar{D}^0 D_s^+)| \approx 1$, and potentially in a large CP asymmetry for \bar{D}^0 decays to CP eigenstates. In contrast, in $B^+ \rightarrow \bar{D}^0 K^+$ decays, the small value of $r_B \equiv |A(B^+ \rightarrow D^0 K^+)/A(B^+ \rightarrow \bar{D}^0 K^+)| \approx 0.1$ results in small values of the CP asymmetry. However, observing and using $B_c^+ \rightarrow D_s^+ \bar{D}^0$ decays is challenging because of the small B_c^+ production cross-section, the short B_c^+ lifetime, the complex final states, and the small branching fractions.

This paper describes a search, performed for the first time, for twelve $B_c^+ \rightarrow D_{(s)}^{(*)+} \bar{D}^{(*)0}$ decay channels, using data collected by the LHCb experiment and corresponding to an integrated luminosity of 3.0 fb^{-1} , of which 1.0 fb^{-1} was recorded at a centre-of-mass energy $\sqrt{s} = 7 \text{ TeV}$ and 2.0 fb^{-1} at $\sqrt{s} = 8 \text{ TeV}$. Charm mesons are reconstructed in the $D^0 \rightarrow K^- \pi^+$, $D^0 \rightarrow K^- \pi^+ \pi^- \pi^+$, $D^+ \rightarrow K^- \pi^+ \pi^+$, and $D_s^+ \rightarrow K^+ K^- \pi^+$ decay modes. For B_c^+ decays that involve one or more excited charm mesons, no attempt is made to reconstruct the low-momentum particles from the decay of excited charm mesons: the distribution of the invariant mass of the partially reconstructed final-state peaks at masses just below the B_c^+ mass.

The branching fractions, \mathcal{B} , of B_c^+ decays to fully reconstructed states are measured relative to high-yield $B^+ \rightarrow D_{(s)}^+ \bar{D}^0$ normalisation modes,

$$\frac{f_c}{f_u} \frac{\mathcal{B}(B_c^+ \rightarrow D_{(s)}^+ \bar{D}^0)}{\mathcal{B}(B^+ \rightarrow D_{(s)}^+ \bar{D}^0)} = \frac{N(B_c^+ \rightarrow D_{(s)}^+ \bar{D}^0)}{N(B^+ \rightarrow D_{(s)}^+ \bar{D}^0)} \frac{\varepsilon(B^+ \rightarrow D_{(s)}^+ \bar{D}^0)}{\varepsilon(B_c^+ \rightarrow D_{(s)}^+ \bar{D}^0)}, \quad (1)$$

where f_c/f_u is the ratio of B_c^+ to B^+ production cross-sections, N stands for the signal yields, and ε for the total efficiencies. For B_c^+ decays with one excited charm meson, the invariant-mass distributions of $B_c^+ \rightarrow D_{(s)}^{*+} \bar{D}^0$ and $B_c^+ \rightarrow D_{(s)}^+ \bar{D}^{*0}$ decays are very similar, and the sum of their branching fractions is measured, weighted by the branching fraction of the excited charged charm meson to a charged charm meson and a low-momentum neutral particle, $\mathcal{B}(D_{(s)}^{*+} \rightarrow D_{(s)}^+ \pi^0, \gamma)$,

$$\begin{aligned} \frac{f_c}{f_u} \frac{\mathcal{B}(B_c^+ \rightarrow D_{(s)}^{*+} \bar{D}^0) \mathcal{B}(D_{(s)}^{*+} \rightarrow D_{(s)}^+ \pi^0, \gamma) + \mathcal{B}(B_c^+ \rightarrow D_{(s)}^+ \bar{D}^{*0})}{\mathcal{B}(B^+ \rightarrow D_{(s)}^+ \bar{D}^0)} = \\ \frac{N(B_c^+ \rightarrow D_{(s)}^{*+} \bar{D}^0) + N(B_c^+ \rightarrow D_{(s)}^+ \bar{D}^{*0})}{N(B^+ \rightarrow D_{(s)}^+ \bar{D}^0)} \frac{\varepsilon(B^+ \rightarrow D_{(s)}^+ \bar{D}^0)}{\varepsilon(B_c^+ \rightarrow D_{(s)}^{*+} \bar{D}^0, D_{(s)}^+ \bar{D}^{*0})}, \end{aligned} \quad (2)$$

where $\varepsilon(B_c^+ \rightarrow D_{(s)}^{*+} \bar{D}^0, D_{(s)}^+ \bar{D}^{*0})$ is the average efficiency of $B_c^+ \rightarrow D_{(s)}^{*+} \bar{D}^0$ and $B_c^+ \rightarrow D_{(s)}^+ \bar{D}^{*0}$ decays. Branching fractions of $B_c^+ \rightarrow D_{(s)}^{*+} \bar{D}^0$ are corrected for $\mathcal{B}(D_{(s)}^{*+} \rightarrow D_{(s)}^+ \pi^0, \gamma)$,

$$\begin{aligned} \frac{f_c}{f_u} \frac{\mathcal{B}(B_c^+ \rightarrow D_{(s)}^{*+} \bar{D}^{*0})}{\mathcal{B}(B^+ \rightarrow D_{(s)}^+ \bar{D}^0)} = \\ \frac{1}{\mathcal{B}(D_{(s)}^{*+} \rightarrow D_{(s)}^+ \pi^0, \gamma)} \frac{N(B_c^+ \rightarrow D_{(s)}^{*+} \bar{D}^{*0})}{N(B^+ \rightarrow D_{(s)}^+ \bar{D}^0)} \frac{\varepsilon(B^+ \rightarrow D_{(s)}^+ \bar{D}^0)}{\varepsilon(B_c^+ \rightarrow D_{(s)}^{*+} \bar{D}^{*0})}. \end{aligned} \quad (3)$$

LHCb measurements of $(f_c \mathcal{B}(B_c^+ \rightarrow J/\psi \pi^+))/(f_u \mathcal{B}(B^+ \rightarrow J/\psi K^+))$ show no significant difference of f_c/f_u between $\sqrt{s} = 7 \text{ TeV}$ [13] and $\sqrt{s} = 8 \text{ TeV}$ [14] in the LHCb acceptance. Predictions for $\mathcal{B}(B_c^+ \rightarrow J/\psi \pi^+)$ range from 6.0×10^{-4} to 2.9×10^{-3} [15–17], implying a value of f_c/f_u in the range 0.24%–1.2%. Since $\mathcal{B}(B_c^+ \rightarrow J/\psi \pi^+)$ is presently not measured, the results in this paper are expressed as the product of f_c/f_u and the ratio of B_c^+ to B^+ branching fractions.

2. Detector and simulation

The LHCb detector [18,19] is a single-arm forward spectrometer covering the pseudorapidity range $2 < \eta < 5$, designed for the study of particles containing b or c quarks. The detector includes a high-precision tracking system consisting of a silicon-strip vertex detector surrounding the pp interaction region [20], a large-area silicon-strip detector located upstream of a dipole magnet with a bending power of about 4 Tm, and three stations of silicon-strip detectors and straw drift tubes [21] placed downstream of the magnet. The polarity of the dipole magnet is reversed periodically throughout data-taking.

The tracking system provides a measurement of the momentum of charged particles with a relative uncertainty that varies from 0.5% at low momentum to 1.0% at 200 GeV/ c . The minimum distance of a track to a primary pp interaction vertex (PV), the impact parameter (IP), is measured with a resolution of $(15 + 29/p_T) \mu\text{m}$, where p_T is the momentum transverse to

the beamline expressed in GeV/c. Different types of charged hadrons are distinguished using information from two ring-imaging Cherenkov detectors [22]. Photons, electrons and hadrons are identified by a calorimeter system consisting of scintillating-pad and preshower detectors, an electromagnetic calorimeter and a hadronic calorimeter. Muons are identified by a system composed of alternating layers of iron and multiwire proportional chambers [23].

The online event selection is performed by a trigger [24], which consists of a hardware stage, based on information from the calorimeter and muon systems, followed by a software stage, which applies a full event reconstruction. At the hardware trigger stage, events are required to have a muon with high p_T or a hadron, photon or electron with high transverse energy in the calorimeters. For hadrons, the transverse energy threshold is about 3.5 GeV. The software trigger requires a two-, three- or four-track secondary vertex with a large sum of the transverse momentum of the tracks and a significant displacement from any PV. At least one track should have $p_T > 1.7$ GeV/c and χ^2_{IP} with respect to any PV greater than 16, where χ^2_{IP} is defined as the difference in the vertex-fit χ^2 of a given PV reconstructed with and without the considered particle. A multivariate algorithm [25] is used for the identification of secondary vertices consistent with the decay of a b hadron.

Simulated events are used for the training of the multivariate selection of the B_c^+ signals, for establishing the shape of the invariant-mass distributions of the signals, and for determining the relative efficiency between the B_c^+ signal decays and the B^+ normalisation modes. In the simulation, pp collisions with $B^+ \rightarrow D_{(s)}^+ \bar{D}^0$ decays are generated using PYTHIA [26] with a specific LHCb configuration [27]. For $B_c^+ \rightarrow D_{(s)}^+ \bar{D}^0$ decays, the BCVEGPY [28] generator is used. The simulated $B_c^+ \rightarrow D_{(s)}^+ \bar{D}^0$ sample is also used for training and efficiency calculations of the $B_c^+ \rightarrow D_{(s)}^+ D^0$ decay mode. Decays of hadronic particles are described by EVTGEN [29], with final-state radiation generated using PHOTOS [30]. The interaction of the generated particles with the detector, and its response, are implemented using the GEANT4 toolkit [31] as described in Ref. [32]. Known discrepancies in the simulation are corrected using data-driven methods.

3. Candidate selection

Initially, loose requirements are made to select candidates having both a $D_{(s)}^+$ and a D^0 or \bar{D}^0 meson. The charm-meson candidates are constructed by combining two, three or four tracks that are incompatible with originating from any reconstructed PV. In addition, the tracks must form a high-quality vertex and the scalar sum of their transverse momenta must exceed 1.8 GeV/c. The pion and kaon candidates are also required to satisfy loose particle identification (PID) criteria to reduce the contribution to the selected sample from misidentified particles. Charm-meson candidates must have an invariant mass within ± 25 MeV/ c^2 of their known value [33]. Using the same method as in Ref. [34], three-track combinations that are compatible with both $D^+ \rightarrow K^- \pi^+ \pi^+$ and $D_s^+ \rightarrow K^+ K^- \pi^+$ decays are categorised as a D_s^+ candidate if the $K^+ K^-$ combination is compatible with the $\phi \rightarrow K^+ K^-$ decay or if the K^+ candidate satisfies strict PID criteria, and as a D^+ candidate otherwise. The two charm mesons are combined into a $B_{(c)}^+$ candidate, which is retained if its invariant mass is in the range 4.8–7.0 GeV/ c^2 . The $D_{(s)}^+ \bar{D}^0$ pair must form a good-quality vertex with transverse momentum exceeding 4.0 GeV/c. The resulting trajectory of the $B_{(c)}^+$ candidate must be consistent with originating from the associated PV, where the associated PV is the PV with which the $B_{(c)}^+$ candidate has the smallest χ^2_{IP} . The reconstructed decay time

divided by its uncertainty, t/σ_t , of D^0 and D_s^+ mesons with respect to the $B_{(c)}^+$ vertex is required to exceed -3 , while that of the longer-lived D^+ meson is required to exceed $+3$. The tighter decay-time significance criterion on the D^+ eliminates background from $B^+ \rightarrow \bar{D}^0 \pi^+ \pi^- \pi^+$ decays where the negatively charged pion is misidentified as a kaon.

The invariant-mass resolution of $B_{(c)}^+$ decays is significantly improved by applying a kinematic fit [35] where the masses of the D^0 and the $D_{(s)}^+$ candidates are fixed to their known values [33], all particles from the $D_{(s)}^+$, D^0 , or $B_{(c)}^+$ decay are constrained to originate from their decay vertex and the $B_{(c)}^+$ is constrained to originate from a PV.

To reduce the combinatorial background, while keeping the efficiency for signal as high as possible, a multivariate selection based on a boosted decision tree (BDT) [36,37] is employed. The following variables are used as input for the BDT: the transverse momentum and the ratio of the likelihood between the kaon and pion PID hypotheses of all final-state particles; the fit quality of the $B_{(c)}^+$ and both charm-meson vertices; the value of χ_{IP}^2 of the $B_{(c)}^+$ candidate; the values of t/σ_t of the $B_{(c)}^+$ and both charm-meson candidates; the invariant masses of the reconstructed charm-meson candidates; and the invariant masses of the pairs of opposite-charge tracks from the $D_{(s)}^+$ candidate.

Four distinct classifiers are constructed: the BDT training is performed separately for the $D_s^+ \bar{D}^0$ and $D^+ \bar{D}^0$ final states and for the $D^0 \rightarrow K^- \pi^+$ and $D^0 \rightarrow K^- \pi^+ \pi^- \pi^+$ decay channels. For a given D^0 final state, the same classifier is used for both $B_c^+ \rightarrow D_{(s)}^+ \bar{D}^0$ and $B_c^+ \rightarrow D_{(s)}^+ D^0$ decays. For signal, the BDT is trained using simulated B_c^+ events, while for background data in the range $5350 < m(D_{(s)}^+ \bar{D}^0) < 6200 \text{ MeV}/c^2$ are used. Studies indicate that the combinatorial background is dominated by non-charm and single-charm candidates, while combinations of two real charm mesons contribute less than 5%. To increase the size of the background sample for the BDT training, the charm mass windows are increased from $\pm 25 \text{ MeV}/c^2$ to $\pm 75 \text{ MeV}/c^2$.

The BDT combines all input variables into a single discriminant. The optimal value of the cut on this discriminant is determined using a procedure based on Ref. [38], maximising $\varepsilon/(\sqrt{N_B} + 5/2)$, where N_B is the expected background in a $\pm 20 \text{ MeV}/c^2$ window around the B_c^+ mass, and the number 5 is the target significance. Simulated events are used to estimate the signal efficiency ε .

4. Data fit

After the selection, a model of the invariant-mass distribution of $B_{(c)}^+ \rightarrow D_{(s)}^+ \bar{D}^0$ candidates is fitted to the data. The model is composed of six components: the signals for fully reconstructed B^+ and B_c^+ decays; the signal for B_c^+ decays with one excited charm meson in the final state; the signal for B_c^+ decays with two excited charm mesons in the final state; the background from $B^+ \rightarrow \bar{D}^0 K^+ K^- \pi^+$ decays; and the combinatorial background.

Fully reconstructed B^+ and B_c^+ signals are described by the sum of two Crystal Ball (CB) [39] functions, with power-law tails proportional to $[m(D_{(s)}^+ \bar{D}^0) - m(B_{(c)}^+)]^{-2}$ in opposite directions. The peak values of both CB components are constrained to be equal and the other shape parameters of the CB functions are obtained from a fit to the simulated events. The peak position of the B^+ signal is a free parameter in the fit to data, while the peak position of the B_c^+ signal is fixed to the world-average measurement [33]. The large $B^+ \rightarrow D_s^+ \bar{D}^0$ signal from data is well described by this model.

Table 2

Ratio $\varepsilon_{B_c^+}/\varepsilon_{B^+}$ of total efficiencies of B_c^+ decays relative to the corresponding fully reconstructed B^+ decays. The quoted uncertainties are statistical only.

Decay channel	Reconstructed state			
	$D_s^+(\overline{D})^0$ with $D^0 \rightarrow$		$D^+(\overline{D})^0$ with $D^0 \rightarrow$	
	$K^-\pi^+$	$K^-\pi^+\pi^-\pi^+$	$K^-\pi^+$	$K^-\pi^+\pi^-\pi^+$
$B_c^+ \rightarrow D_{(s)}^+(\overline{D})^0$	0.420 ± 0.005	0.373 ± 0.009	0.441 ± 0.007	0.398 ± 0.010
$B_c^+ \rightarrow D_{(s)}^{*+}(\overline{D})^0, D_{(s)}^+(\overline{D})^{*0}$	0.372 ± 0.006	0.317 ± 0.010	0.381 ± 0.008	0.337 ± 0.011
$B_c^+ \rightarrow D_{(s)}^{*+}(\overline{D})^{*0}$	0.339 ± 0.006	0.278 ± 0.009	0.342 ± 0.007	0.297 ± 0.010

Models for decays where one or two low-momentum particles from excited charm-meson decays are missing are implemented as templates, obtained from invariant-mass distributions of simulated data. For decays with one missing low-momentum particle, both $B_c^+ \rightarrow D_{(s)}^{*+}(\overline{D})^0$ and $B_c^+ \rightarrow D_{(s)}^+(\overline{D})^{*0}$ decays contribute and the template is based on the sum of the two decay modes, weighted by the appropriate branching fractions of the excited charm mesons. For $B_c^+ \rightarrow D_{(s)}^{*+}(\overline{D})^{*0}$ decays, it is assumed that both excited charm mesons are produced unpolarised.

The Cabibbo-favoured $B^+ \rightarrow \overline{D}^0 K^+ K^- \pi^+$ decay is a background to the $B^+ \rightarrow D_s^+ \overline{D}^0$ channel, though its yield is strongly reduced by the charm-meson mass requirement. This background is modelled by a single Gaussian function, with the width determined from a sample of simulated decays and the normalisation determined from the sidebands of the D_s^+ mass peak. The yield of this background is about 40 times smaller than that of the signal, and the shape of the invariant-mass distribution is twice as wide. The combinatorial background is described by the sum of an exponential function and a constant.

An unbinned extended maximum likelihood fit is used to simultaneously describe the invariant-mass distributions of candidates with $D^0 \rightarrow K^- \pi^+$ and $D^0 \rightarrow K^- \pi^+ \pi^- \pi^+$ decays, resulting in four independent fits to eight invariant mass distributions. In these fits the background parameters and B^+ yields are free to vary independently, but the ratio of the B_c^+ yields for the two D^0 decay modes is constrained to the corresponding ratio of B^+ yields, corrected for the relative efficiencies. The total B_c^+ yield, $N_{B_c^+}^{\text{tot}}$, is a free parameter in these fits, leading to a B_c^+ yield in each data sample given by the expressions

$$N_{B_c^+}^{K\pi} = \frac{N_{B^+}^{K\pi} \varepsilon_{B_c^+}^{K\pi} / \varepsilon_{B^+}^{K\pi}}{N_{B^+}^{K\pi} \varepsilon_{B_c^+}^{K\pi} / \varepsilon_{B^+}^{K\pi} + N_{B^+}^{K\pi\pi\pi} \varepsilon_{B_c^+}^{K\pi\pi\pi} / \varepsilon_{B^+}^{K\pi\pi\pi}} N_{B_c^+}^{\text{tot}}, \quad (4)$$

$$N_{B_c^+}^{K\pi\pi\pi} = \frac{N_{B^+}^{K\pi\pi\pi} \varepsilon_{B_c^+}^{K\pi\pi\pi} / \varepsilon_{B^+}^{K\pi\pi\pi}}{N_{B^+}^{K\pi} \varepsilon_{B_c^+}^{K\pi} / \varepsilon_{B^+}^{K\pi} + N_{B^+}^{K\pi\pi\pi} \varepsilon_{B_c^+}^{K\pi\pi\pi} / \varepsilon_{B^+}^{K\pi\pi\pi}} N_{B_c^+}^{\text{tot}}. \quad (5)$$

The relative efficiencies that appear in these expressions, calculated for simulated events generated in the rapidity range $2.0 < y(B_{(c)}^+) < 4.5$ and with $p_T(B_{(c)}^+) > 4 \text{ GeV}/c$, are summarised in Table 2.

The results of the fits are shown in Fig. 2, and the corresponding signal yields are listed in Table 3. The small peaks at the B^+ mass in the $D_{(s)}^+ \overline{D}^0$ final state are due to $B^+ \rightarrow D_{(s)}^+ \overline{D}^0$ decays either followed by the doubly Cabibbo-suppressed $D^0 \rightarrow K^+ \pi^-$ decay or when both the

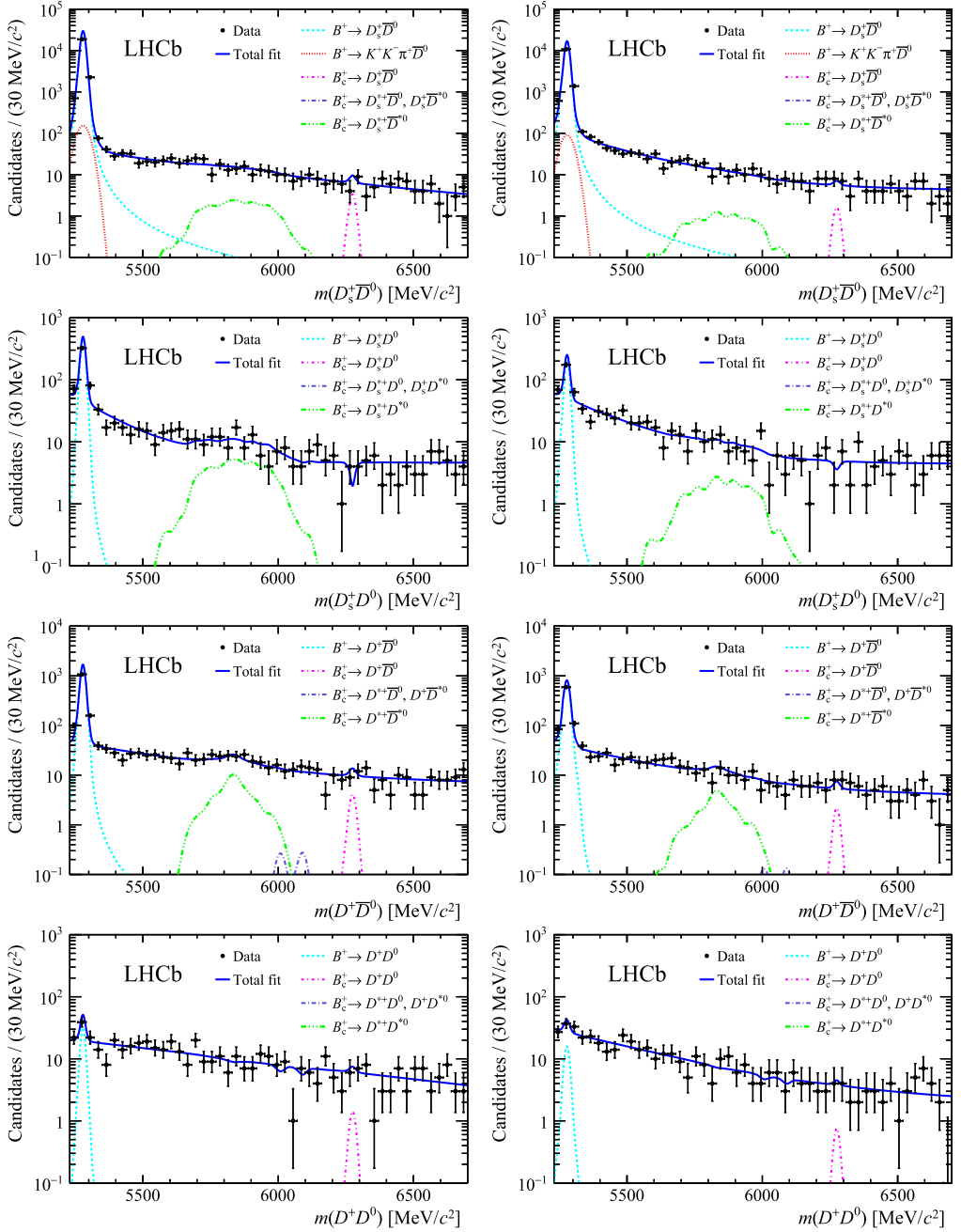


Fig. 2. Fits to the (top row) $D_s^+ \bar{D}^0$, (second row) $D_s^+ D^0$, (third row) $D^+ \bar{D}^0$ and (bottom row) $D^+ D^0$ final states. For the left plots, the D^0 meson is reconstructed in the $K^- \pi^+$ final state, while the right column corresponds to the $D^0 \rightarrow K^- \pi^+ \pi^- \pi^+$ mode.

Table 3

Signal yields from the fits of $B \rightarrow D_{(s)}^+ (\overline{D})^0$ decays. Samples with $D^0 \rightarrow K^- \pi^+$ and $D^0 \rightarrow K^- \pi^+ \pi^- \pi^+$ are fitted simultaneously. The uncertainties are statistical only.

Decay channel	Reconstructed state			
	$D_s^+ \overline{D}^0$	$D_s^+ D^0$	$D^+ \overline{D}^0$	$D^+ D^0$
$B^+ \rightarrow D_{(s)}^+ \overline{D}^0$	$33\,734 \pm 187$	476 ± 27	1866 ± 46	37 ± 11
$B_c^+ \rightarrow D_{(s)}^+ (\overline{D})^0$	5 ± 5	-4 ± 3	6 ± 6	2 ± 4
$B_c^+ \rightarrow D_{(s)}^{*+} (\overline{D})^0, D_{(s)}^+ (\overline{D})^{*0}$	-1 ± 14	-4 ± 10	1 ± 13	-10 ± 9
$B_c^+ \rightarrow D_{(s)}^{*+} (\overline{D})^{*0}$	34 ± 28	73 ± 19	68 ± 23	-8 ± 14

Table 4

Systematic uncertainties on the B_c^+ yields, for the combined fit to both the $D^0 \rightarrow K^- \pi^+$ and the $D^0 \rightarrow K^- \pi^+ \pi^- \pi^+$ decay channels. The total systematic uncertainty is calculated as the quadratic sum of the individual components.

Source	Reconstructed state			
	$D_s^+ \overline{D}^0$	$D_s^+ D^0$	$D^+ \overline{D}^0$	$D^+ D^0$
$B_c^+ \rightarrow D_{(s)}^+ (\overline{D})^0$				
Signal shape	0.25	0.28	0.31	0.13
Signal model	0.40	0.34	0.61	0.44
B_c^+ mass	0.64	0.62	0.79	0.51
Background model	1.12	1.75	1.88	0.56
Fit bias	0.70	1.28	0.27	0.19
Total	1.54	2.30	2.17	0.91
$B_c^+ \rightarrow D_{(s)}^{*+} (\overline{D})^0, D_{(s)}^+ (\overline{D})^{*0}$				
Signal composition	7.6	5.5	7.1	5.7
Background model	11.9	17.5	16.4	4.5
Fit bias	5.5	9.4	3.9	1.3
Total	15.2	20.6	18.3	7.4
$B_c^+ \rightarrow D_{(s)}^{*+} (\overline{D})^{*0}$				
Polarisation	23	14	9	5
Background model	43	98	37	9
Fit bias	10	7	8	1
Total	49	99	39	10

kaon and pion are misidentified. No significant B_c^+ signals are observed; after taking into account systematic uncertainties, discussed in Sec. 5, none of the signals exceeds a significance of two standard deviations, which is measured as the difference in likelihood when fitting the data with or without signal component in the fit [40].

5. Systematic uncertainties

The systematic uncertainties on the B_c^+ yields are listed in Table 4 and described below. The signal shape parameters for the fully reconstructed modes are varied according to Gaussian distributions that take into account the covariance matrix of the fit to the simulated events, and

Table 5

Systematic uncertainties, in %, on the normalisation of the B_c^+ branching fraction determination. The total systematic uncertainty is calculated as the quadratic sum of the individual components.

Channel	Source	Reconstructed state			
		$D_s^+ \bar{D}^0$, with $D^0 \rightarrow$		$D^+ \bar{D}^0$, with $D^0 \rightarrow$	
		$K^- \pi^+$	$K^- \pi^+ \pi^- \pi^+$	$K^- \pi^+$	$K^- \pi^+ \pi^- \pi^+$
Common	B^+ stat.	0.7	0.9	3.1	4.3
	B^+ signal shape	0.0	0.0	0.0	0.3
	B^+ signal model	0.1	0.2	0.1	0.3
	Background model	0.0	0.6	1.6	1.3
	$B^+ \rightarrow \bar{D}^0 K^+ K^- \pi^+$	1.4	1.4	–	–
	B_c^+ lifetime	1.5	1.5	1.5	1.5
	PID	2.4	0.9	1.2	3.2
	D^0 model	–	1.1	–	0.7
$B_c^+ \rightarrow D_{(s)}^+ \bar{D}^0$	Simulation stat.	1.2	2.4	1.6	2.5
	Total	3.5	3.6	4.3	6.3
$B_c^+ \rightarrow D_{(s)}^{*+} \bar{D}^0, D_{(s)}^+ \bar{D}^{*0}$	Simulation stat.	1.7	3.3	2.0	3.3
	Signal composition	1.0	0.8	0.7	2.6
	Total	3.8	4.3	4.5	7.1
$B_c^+ \rightarrow D_{(s)}^{*+} \bar{D}^{*0}$	Simulation stat.	1.7	3.4	2.0	3.3
	Polarisation	1.5	0.4	1.4	1.3
	$\mathcal{B}(D^{*+} \rightarrow D^+ \pi^0, \gamma)$	–	–	1.5	1.5
	Total	3.9	4.4	4.9	6.9

evaluating the change in yield and its uncertainty for 1000 variations. An additional uncertainty is attributed to the signal model by changing its description from a sum of two CB functions to a sum of two Gaussian functions. The assumed peak position of the $B_c^+ \rightarrow D_{(s)}^+ \bar{D}^0$ signal may differ from the true value. This is taken into account by varying the B_c^+ peak position by its uncertainty, taken as the squared sum of uncertainty on the world-average B_c^+ mass ($0.8 \text{ MeV}/c^2$) and the contribution from the LHCb momentum-scale uncertainty ($0.8 \text{ MeV}/c^2$) [41]. The signal shape of the decays with one missing low-momentum particle is based on the assumption $\mathcal{B}(B_c^+ \rightarrow D_{(s)}^{*+} \bar{D}^0) = \mathcal{B}(B_c^+ \rightarrow D_{(s)}^+ \bar{D}^{*0})$. Since the B_c^+ branching fractions are unknown, the signal composition is varied using $B_c^+ \rightarrow D_{(s)}^{*+} \bar{D}^0$ or $B_c^+ \rightarrow D_{(s)}^+ \bar{D}^{*0}$ only and the largest difference is taken as the systematic uncertainty. As the polarisation of excited charm mesons in $B_c^+ \rightarrow D_{(s)}^{*+} \bar{D}^{*0}$ decays is unknown, the signal shapes are varied between fully longitudinal and fully transverse polarisations, and the largest yield difference with the unpolarised decay model is taken as the uncertainty. To evaluate the uncertainty in the choice of the shape of the combinatorial background, an alternative fit is applied using an exponential function to model the background. To evaluate eventual biases of the B_c^+ yields in the fit, pseudoexperiments are generated where the candidates in the signal window are replaced by the expected distribution using only background. The yields are corrected for this bias and the attributed uncertainty is the squared sum of the bias and its statistical uncertainty.

Systematic uncertainties that affect the normalisation are listed in Table 5 and are described below. The limited size of the simulated signal samples affects the normalisation as well as the

statistical uncertainties of the B^+ yields. The systematic uncertainties of the B^+ yields are evaluated by varying the signal shape according to the covariance matrix of the fit to simulated data and by changing the signal model to the sum of two Gaussian functions. The B^+ yield is also affected by uncertainties on the background, which are evaluated by changing the background shape to an exponential function and by varying the single-charm background by 100% of its yield. The impact on the efficiency ratio of the uncertainty on the B_c^+ lifetime is evaluated by changing its lifetime by one standard deviation. Imperfections in the rescaling of the PID variables [22] are quantified by considering the efficiency ratio with and without PID corrections and assigning the difference as a systematic uncertainty. The $D^0 \rightarrow K^-\pi^+\pi^-\pi^+$ decay has a complicated substructure, but was simulated according to a phase-space model. The systematic uncertainty is taken as the quadratic sum of the differences in efficiency ratio when the simulated events are weighted to reproduce the $\pi^+\pi^-$, $K^-\pi^+$, $K^-\pi^+\pi^-$ and $\pi^+\pi^-\pi^+$ invariant-mass distributions observed in data. The difference in efficiency when applying the model variations for B_c^+ decays with one or two excited charm mesons in the final state is taken into account as a systematic uncertainty. The determinations of the $B_c^+ \rightarrow D^{*+}\bar{D}^{*0}$ branching fraction ratios are corrected for $\mathcal{B}(D^{*+} \rightarrow D^+\pi^0, \gamma) = (32.3 \pm 0.5)\%$ [33], as is indicated in Eq. (3), and the corresponding uncertainty is assigned as a systematic uncertainty.

6. Results and conclusion

To determine the branching fraction ratios, fits to data are performed where the free parameters are not the individual yields, but correspond to the left-hand-side terms of Eqs. (1)–(3). In these fits, the systematic uncertainties are taken into account as Gaussian constraints.

The measured branching fraction ratios for the fully reconstructed B_c^+ decays are listed below. Quoted in brackets are the corresponding upper limits calculated at 90% (95%) confidence level with the asymptotic CL_s method [42],

$$\begin{aligned} \frac{f_c}{f_u} \frac{\mathcal{B}(B_c^+ \rightarrow D_s^+\bar{D}^0)}{\mathcal{B}(B^+ \rightarrow D_s^+\bar{D}^0)} &= (3.0 \pm 3.7) \times 10^{-4} [< 0.9 (1.1) \times 10^{-3}], \\ \frac{f_c}{f_u} \frac{\mathcal{B}(B_c^+ \rightarrow D_s^+D^0)}{\mathcal{B}(B^+ \rightarrow D_s^+\bar{D}^0)} &= (-3.8 \pm 2.6) \times 10^{-4} [< 3.7 (4.7) \times 10^{-4}], \\ \frac{f_c}{f_u} \frac{\mathcal{B}(B_c^+ \rightarrow D^+\bar{D}^0)}{\mathcal{B}(B^+ \rightarrow D^+\bar{D}^0)} &= (8.0 \pm 7.5) \times 10^{-3} [< 1.9 (2.2) \times 10^{-2}], \\ \frac{f_c}{f_u} \frac{\mathcal{B}(B_c^+ \rightarrow D^+D^0)}{\mathcal{B}(B^+ \rightarrow D^+\bar{D}^0)} &= (2.9 \pm 5.3) \times 10^{-3} [< 1.2 (1.4) \times 10^{-2}]. \end{aligned}$$

For B_c^+ decays with one excited charm meson, the results are

$$\begin{aligned} \frac{f_c}{f_u} \frac{\mathcal{B}(B_c^+ \rightarrow D_s^{*+}\bar{D}^0) + \mathcal{B}(B_c^+ \rightarrow D_s^+\bar{D}^{*0})}{\mathcal{B}(B^+ \rightarrow D_s^+\bar{D}^0)} &= \\ &= (-0.1 \pm 1.5) \times 10^{-3} [< 2.8 (3.4) \times 10^{-3}], \\ \frac{f_c}{f_u} \frac{\mathcal{B}(B_c^+ \rightarrow D_s^{*+}D^0) + \mathcal{B}(B_c^+ \rightarrow D_s^+D^{*0})}{\mathcal{B}(B^+ \rightarrow D_s^+\bar{D}^0)} &= \\ &= (-0.3 \pm 1.9) \times 10^{-3} [< 3.0 (3.6) \times 10^{-3}], \end{aligned}$$

$$\frac{f_c}{f_u} \frac{\mathcal{B}(B_c^+ \rightarrow (D^{*+} \rightarrow D^+ \pi^0, \gamma) \bar{D}^0) + \mathcal{B}(B_c^+ \rightarrow D^+ \bar{D}^{*0})}{\mathcal{B}(B^+ \rightarrow D^+ \bar{D}^0)} =$$

$$(0.2 \pm 3.2) \times 10^{-2} [< 5.5 (6.6) \times 10^{-2}],$$

$$\frac{f_c}{f_u} \frac{\mathcal{B}(B_c^+ \rightarrow (D^{*+} \rightarrow D^+ \pi^0, \gamma) D^0) + \mathcal{B}(B_c^+ \rightarrow D^+ D^{*0})}{\mathcal{B}(B^+ \rightarrow D^+ \bar{D}^0)} =$$

$$(-1.5 \pm 1.7) \times 10^{-2} [< 2.2 (2.8) \times 10^{-2}].$$

For B_c^+ decays with two excited charm mesons, the measurements give

$$\frac{f_c}{f_u} \frac{\mathcal{B}(B_c^+ \rightarrow D_s^{*+} \bar{D}^{*0})}{\mathcal{B}(B^+ \rightarrow D_s^+ \bar{D}^0)} = (3.2 \pm 4.3) \times 10^{-3} [< 1.1 (1.3) \times 10^{-2}],$$

$$\frac{f_c}{f_u} \frac{\mathcal{B}(B_c^+ \rightarrow D_s^{*+} D^{*0})}{\mathcal{B}(B^+ \rightarrow D_s^+ \bar{D}^0)} = (7.0 \pm 9.2) \times 10^{-3} [< 2.0 (2.4) \times 10^{-2}],$$

$$\frac{f_c}{f_u} \frac{\mathcal{B}(B_c^+ \rightarrow D^{*+} \bar{D}^{*0})}{\mathcal{B}(B^+ \rightarrow D^+ \bar{D}^0)} = (3.4 \pm 2.3) \times 10^{-1} [< 6.5 (7.3) \times 10^{-1}],$$

$$\frac{f_c}{f_u} \frac{\mathcal{B}(B_c^+ \rightarrow D^{*+} D^{*0})}{\mathcal{B}(B^+ \rightarrow D^+ \bar{D}^0)} = (-4.1 \pm 9.1) \times 10^{-2} [< 1.3 (1.6) \times 10^{-1}].$$

The presented limits are consistent with the theoretical expectations: assuming a value of $f_c/f_u = 1.2\%$, the branching fraction ratio limits give $\mathcal{B}(B_c^+ \rightarrow D^+ \bar{D}^0) < 6.0 (7.0) \times 10^{-4}$ at 90% (95%) confidence level, well above the values shown in Table 1.

Acknowledgements

We express our gratitude to our colleagues in the CERN accelerator departments for the excellent performance of the LHC. We thank the technical and administrative staff at the LHCb institutes. We acknowledge support from CERN and from the national agencies: CAPES, CNPq, FAPERJ and FINEP (Brazil); MOST and NSFC (China); CNRS/IN2P3 (France); BMBF, DFG and MPG (Germany); INFN (Italy); NWO (The Netherlands); MNiSW and NCN (Poland); MEN/IFA (Romania); MinES and FASO (Russia); MINECO (Spain); SNSF and SER (Switzerland); NASU (Ukraine); STFC (United Kingdom); NSF (USA). We acknowledge the computing resources that are provided by CERN, IN2P3 (France), KIT and DESY (Germany), INFN (Italy), SURF (The Netherlands), PIC (Spain), GridPP (United Kingdom), RRCKI and Yandex LLC (Russia), CSCS (Switzerland), IFIN-HH (Romania), CBPF (Brazil), PL-GRID (Poland) and OSC (USA). We are indebted to the communities behind the multiple open-source software packages on which we depend. Individual groups or members have received support from AvH Foundation (Germany), EPLANET, Marie Skłodowska-Curie Actions and ERC (European Union), ANR, Labex P2IO and OCEVU, and Région Auvergne-Rhône-Alpes (France), RFBR, RSF and Yandex LLC (Russia), GVA, XuntaGal and GENCAT (Spain), Herchel Smith Fund, the Royal Society, the English-Speaking Union and the Leverhulme Trust (United Kingdom).

References

- [1] N. Cabibbo, Unitary symmetry and leptonic decays, *Phys. Rev. Lett.* **10** (1963) 531.
- [2] M. Kobayashi, T. Maskawa, CP violation in the renormalizable theory of weak interaction, *Prog. Theor. Phys.* **49** (1973) 652.

- [3] LHCb Collaboration, R. Aaij, et al., Measurement of CP observables in $B^\pm \rightarrow D^{(*)}K^\pm$ and $B^\pm \rightarrow D^{(*)}\pi^\pm$ decays, *Phys. Lett. B* 777 (2018) 16–30, arXiv:1708.06370.
- [4] LHCb Collaboration, R. Aaij, et al., Measurement of the CKM angle γ from a combination of LHCb results, *J. High Energy Phys.* 12 (2016) 087, arXiv:1611.03076.
- [5] M. Masetti, CP violation in B_c^+ decays, *Phys. Lett. B* 286 (1992) 160.
- [6] R. Fleischer, D. Wyler, Exploring CP violation with B_c^+ decays, *Phys. Rev. D* 62 (2000) 057503, arXiv:hep-ph/0004010.
- [7] A.K. Giri, R. Mohanta, M.P. Khanna, Determination of the angle γ from nonleptonic $B_c^+ \rightarrow D_{(s)}D^0$ decays, *Phys. Rev. D* 65 (2002) 034016, arXiv:hep-ph/0104009.
- [8] A.K. Giri, B. Mawlong, R. Mohanta, Determining the CKM angle γ with B_c^+ decays, *Phys. Rev. D* 75 (2007) 097304, *Phys. Rev. D* 76 (2007) 099902 (Erratum), arXiv:hep-ph/0611212.
- [9] Z. Rui, Z. Zhitian, C.-D. Lu, The double charm decays of B_c meson in the perturbative QCD approach, *Phys. Rev. D* 86 (2012) 074019, arXiv:1203.2303.
- [10] V.V. Kiselev, Exclusive decays and lifetime of B_c meson in QCD sum rules, arXiv:hep-ph/0211021.
- [11] M.A. Ivanov, J.G. Korner, O.N. Pakhomova, The nonleptonic decays $B_c^+ \rightarrow D_s^+ \bar{D}^0$ and $B_c^+ \rightarrow D_s^+ D^0$ in a relativistic quark model, *Phys. Lett. B* 555 (2003) 189, arXiv:hep-ph/0212291.
- [12] M.A. Ivanov, J.G. Korner, P. Santorelli, Exclusive semileptonic and nonleptonic decays of the B_c meson, *Phys. Rev. D* 73 (2006) 054024, arXiv:hep-ph/0602050.
- [13] LHCb Collaboration, R. Aaij, et al., Measurements of B_c^+ production and mass with the $B_c^+ \rightarrow J/\psi\pi^+$ decay, *Phys. Rev. Lett.* 109 (2012) 232001, arXiv:1209.5634.
- [14] LHCb Collaboration, R. Aaij, et al., Measurement of B_c^+ production at $\sqrt{s} = 8\text{ TeV}$, *Phys. Rev. Lett.* 114 (2015) 132001, arXiv:1411.2943.
- [15] D. Ebert, R.N. Faustov, V.O. Galkin, Weak decays of the B_c meson to charmonium and D mesons in the relativistic quark model, *Phys. Rev. D* 68 (2003) 094020, arXiv:hep-ph/0306306.
- [16] C.-H. Chang, Y.-Q. Chen, Decays of the B_c meson, *Phys. Rev. D* 49 (1994) 3399.
- [17] C.-F. Qiao, P. Sun, D. Yang, R.-L. Zhu, B_c exclusive decays to charmonium and a light meson at next-to-leading order accuracy, *Phys. Rev. D* 89 (2014) 034008, arXiv:1209.5859.
- [18] LHCb Collaboration, A.A. Alves Jr., et al., The LHCb detector at the LHC, *J. Instrum.* 3 (2008) S08005.
- [19] LHCb Collaboration, R. Aaij, et al., LHCb detector performance, *Int. J. Mod. Phys. A* 30 (2015) 1530022, arXiv:1412.6352.
- [20] R. Aaij, et al., Performance of the LHCb Vertex Locator, *J. Instrum.* 9 (2014) P09007, arXiv:1405.7808.
- [21] R. Arink, et al., Performance of the LHCb Outer Tracker, *J. Instrum.* 9 (2014) P01002, arXiv:1311.3893.
- [22] M. Adinolfi, et al., Performance of the LHCb RICH detector at the LHC, *Eur. Phys. J. C* 73 (2013) 2431, arXiv:1211.6759.
- [23] A.A. Alves Jr., et al., Performance of the LHCb muon system, *J. Instrum.* 8 (2013) P02022, arXiv:1211.1346.
- [24] R. Aaij, et al., The LHCb trigger and its performance in 2011, *J. Instrum.* 8 (2013) P04022, arXiv:1211.3055.
- [25] V.V. Gligorov, M. Williams, Efficient, reliable and fast high-level triggering using a bonsai boosted decision tree, *J. Instrum.* 8 (2013) P02013, arXiv:1210.6861.
- [26] T. Sjöstrand, S. Mrenna, P. Skands, A brief introduction to PYTHIA 8.1, *Comput. Phys. Commun.* 178 (2008) 852, arXiv:0710.3820;
T. Sjöstrand, S. Mrenna, P. Skands, PYTHIA 6.4 physics and manual, *J. High Energy Phys.* 05 (2006) 026, arXiv:hep-ph/0603175.
- [27] I. Belyaev, et al., Handling of the generation of primary events in Gauss, the LHCb simulation framework, *J. Phys. Conf. Ser.* 331 (2011) 032047.
- [28] C.-H. Chang, C. Driouchi, P. Eerola, X.G. Wu, BCVEGPy: an event generator for hadronic production of the B_c meson, *Comput. Phys. Commun.* 159 (2004) 192, arXiv:hep-ph/0309120.
- [29] D.J. Lange, The EvtGen particle decay simulation package, *Nucl. Instrum. Methods A* 462 (2001) 152.
- [30] P. Golonka, Z. Was, PHOTOS Monte Carlo: a precision tool for QED corrections in Z and W decays, *Eur. Phys. J. C* 45 (2006) 97, arXiv:hep-ph/0506026.
- [31] Geant4 Collaboration, J. Allison, et al., Geant4 developments and applications, *IEEE Trans. Nucl. Sci.* 53 (2006) 270;
Geant4 Collaboration, S. Agostinelli, et al., Geant4: a simulation toolkit, *Nucl. Instrum. Methods A* 506 (2003) 250.
- [32] M. Clemencic, et al., The LHCb simulation application, Gauss: design, evolution and experience, *J. Phys. Conf. Ser.* 331 (2011) 032023.
- [33] Particle Data Group, C. Patrignani, et al., Review of particle physics, *Chin. Phys. C* 40 (2016) 100001, and 2017 update.

- [34] LHCb Collaboration, R. Aaij, et al., Study of beauty hadron decays into pairs of charm hadrons, *Phys. Rev. Lett.* 112 (2014) 202001, arXiv:1403.3606.
- [35] W.D. Hulsbergen, Decay chain fitting with a Kalman filter, *Nucl. Instrum. Methods A* 552 (2005) 566, arXiv:physics/0503191.
- [36] L. Breiman, J.H. Friedman, R.A. Olshen, C.J. Stone, *Classification and Regression Trees*, Wadsworth International Group, Belmont, CA, USA, 1984.
- [37] B.P. Roe, et al., Boosted decision trees as an alternative to artificial neural networks for particle identification, *Nucl. Instrum. Methods A* 543 (2005) 577, arXiv:physics/0408124.
- [38] G. Punzi, Sensitivity of searches for new signals and its optimization, in: L. Lyons, R. Mount, R. Reitmeyer (Eds.), *Statistical Problems in Particle Physics, Astrophysics, and Cosmology*, 2003, p. 79, arXiv:physics/0308063.
- [39] T. Skwarnicki, *A Study of the Radiative Cascade Transitions Between the Upsilon-Prime and Upsilon Resonances*, PhD thesis, Institute of Nuclear Physics, Krakow, 1986, DESY-F31-86-02.
- [40] S.S. Wilks, The large-sample distribution of the likelihood ratio for testing composite hypotheses, *Ann. Math. Stat.* 9 (1938) 60.
- [41] LHCb Collaboration, R. Aaij, et al., Measurements of the Λ_b^0 , Ξ_b^- , and Ω_b^- baryon masses, *Phys. Rev. Lett.* 110 (2013) 182001, arXiv:1302.1072.
- [42] A.L. Read, Presentation of search results: the CL_s technique, *J. Phys. G* 28 (2002) 2693.

LHCb Collaboration

R. Aaij⁴⁰, B. Adeva³⁹, M. Adinolfi⁴⁸, Z. Ajaltouni⁵, S. Akar⁵⁹, J. Albrecht¹⁰, F. Alessio⁴⁰, M. Alexander⁵³, A. Alfonso Albero³⁸, S. Ali⁴³, G. Alkhazov³¹, P. Alvarez Cartelle⁵⁵, A.A. Alves Jr⁵⁹, S. Amato², S. Amerio²³, Y. Amhis⁷, L. An³, L. Anderlini¹⁸, G. Andreassi⁴¹, M. Andreotti^{17,g}, J.E. Andrews⁶⁰, R.B. Appleby⁵⁶, F. Archilli⁴³, P. d'Argent¹², J. Arnau Romeu⁶, A. Artamonov³⁷, M. Artuso⁶¹, E. Aslanides⁶, M. Atzeni⁴², G. Auriemma²⁶, M. Baalouch⁵, I. Babuschkin⁵⁶, S. Bachmann¹², J.J. Back⁵⁰, A. Badalov^{38,m}, C. Baesso⁶², S. Baker⁵⁵, V. Balagura^{7,b}, W. Baldini¹⁷, A. Baranov³⁵, R.J. Barlow⁵⁶, C. Barschel⁴⁰, S. Barsuk⁷, W. Barter⁵⁶, F. Baryshnikov³², V. Batozskaya²⁹, V. Battista⁴¹, A. Bay⁴¹, L. Beaucourt⁴, J. Beddow⁵³, F. Bedeschi²⁴, I. Bediaga¹, A. Beiter⁶¹, L.J. Bel⁴³, N. Beliy⁶³, V. Bellee⁴¹, N. Belloli^{21,i}, K. Belous³⁷, I. Belyaev^{32,40}, E. Ben-Haim⁸, G. Bencivenni¹⁹, S. Benson⁴³, S. Beranek⁹, A. Berezhnoy³³, R. Bernet⁴², D. Berninghoff¹², E. Bertholet⁸, A. Bertolin²³, C. Betancourt⁴², F. Betti¹⁵, M.O. Bettler⁴⁰, M. van Beuzekom⁴³, Ia. Bezshyiko⁴², S. Bifani⁴⁷, P. Billoir⁸, A. Birnkraut¹⁰, A. Bizzeti^{18,u}, M. Bjørn⁵⁷, T. Blake⁵⁰, F. Blanc⁴¹, S. Blusk⁶¹, V. Bocci²⁶, T. Boettcher⁵⁸, A. Bondar^{36,w}, N. Bondar³¹, I. Bordyuzhin³², S. Borghi^{56,40}, M. Borisyak³⁵, M. Borsato³⁹, F. Bossu⁷, M. Boubdir⁹, T.J.V. Bowcock⁵⁴, E. Bowen⁴², C. Bozzi^{17,40}, S. Braun¹², J. Brodzicka²⁷, D. Brundu¹⁶, E. Buchanan⁴⁸, C. Burr⁵⁶, A. Bursche^{16,f}, J. Buytaert⁴⁰, W. Byczynski⁴⁰, S. Cadeddu¹⁶, H. Cai⁶⁴, R. Calabrese^{17,g},

R. Calladine⁴⁷, M. Calvi^{21,i}, M. Calvo Gomez^{38,m}, A. Camboni^{38,m},
 P. Campana¹⁹, D.H. Campora Perez⁴⁰, L. Capriotti⁵⁶, A. Carbone^{15,e},
 G. Carboni^{25,j}, R. Cardinale^{20,h}, A. Cardini¹⁶, P. Carniti^{21,i}, L. Carson⁵²,
 K. Carvalho Akiba², G. Casse⁵⁴, L. Cassina²¹, M. Cattaneo⁴⁰,
 G. Cavallero^{20,40,h}, R. Cenci^{24,t}, D. Chamont⁷, M.G. Chapman⁴⁸,
 M. Charles⁸, Ph. Charpentier⁴⁰, G. Chatzikonstantinidis⁴⁷,
 M. Chefdeville⁴, S. Chen¹⁶, S.F. Cheung⁵⁷, S.-G. Chitic⁴⁰,
 V. Chobanova³⁹, M. Chrzaszcz⁴², A. Chubykin³¹, P. Ciambone¹⁹,
 X. Cid Vidal³⁹, G. Ciezarek⁴⁰, P.E.L. Clarke⁵², M. Clemencic⁴⁰,
 H.V. Cliff⁴⁹, J. Closier⁴⁰, V. Coco⁴⁰, J. Cogan⁶, E. Cogneras⁵,
 V. Cogoni^{16,f}, L. Cojocariu³⁰, P. Collins⁴⁰, T. Colombo⁴⁰,
 A. Comerma-Montells¹², A. Contu¹⁶, G. Coombs⁴⁰, S. Coquereau³⁸,
 G. Corti⁴⁰, M. Corvo^{17,g}, C.M. Costa Sobral⁵⁰, B. Couturier⁴⁰,
 G.A. Cowan⁵², D.C. Craik⁵⁸, A. Crocombe⁵⁰, M. Cruz Torres¹,
 R. Currie⁵², C. D'Ambrosio⁴⁰, F. Da Cunha Marinho², C.L. Da Silva⁷²,
 E. Dall'Occo⁴³, J. Dalseno⁴⁸, A. Davis³, O. De Aguiar Francisco⁴⁰,
 K. De Bruyn⁴⁰, S. De Capua⁵⁶, M. De Cian¹², J.M. De Miranda¹,
 L. De Paula², M. De Serio^{14,d}, P. De Simone¹⁹, C.T. Dean⁵³,
 D. Decamp⁴, L. Del Buono⁸, H.-P. Dembinski¹¹, M. Demmer¹⁰,
 A. Dendek²⁸, D. Derkach³⁵, O. Deschamps⁵, F. Dettori⁵⁴, B. Dey⁶⁵,
 A. Di Canto⁴⁰, P. Di Nezza¹⁹, H. Dijkstra⁴⁰, F. Dordei⁴⁰, M. Dorigo⁴⁰,
 A. Dosil Suárez³⁹, L. Douglas⁵³, A. Dovbnya⁴⁵, K. Dreimanis⁵⁴,
 L. Dufour⁴³, G. Dujany⁸, P. Durante⁴⁰, J.M. Durham⁷², D. Dutta⁵⁶,
 R. Dzhelyadin³⁷, M. Dziewiecki¹², A. Dziurda⁴⁰, A. Dzyuba³¹,
 S. Easo⁵¹, M. Ebert⁵², U. Egede⁵⁵, V. Egorychev³², S. Eidelman^{36,w},
 S. Eisenhardt⁵², U. Eitschberger¹⁰, R. Ekelhof¹⁰, L. Eklund⁵³, S. Ely⁶¹,
 S. Esen¹², H.M. Evans⁴⁹, T. Evans⁵⁷, A. Falabella¹⁵, N. Farley⁴⁷,
 S. Farry⁵⁴, D. Fazzini^{21,i}, L. Federici²⁵, D. Ferguson⁵², G. Fernandez³⁸,
 P. Fernandez Declara⁴⁰, A. Fernandez Prieto³⁹, F. Ferrari¹⁵,
 L. Ferreira Lopes⁴¹, F. Ferreira Rodrigues², M. Ferro-Luzzi⁴⁰,
 S. Filippov³⁴, R.A. Fini¹⁴, M. Fiorini^{17,g}, M. Firlej²⁸, C. Fitzpatrick⁴¹,
 T. Fiutowski²⁸, F. Fleuret^{7,b}, M. Fontana^{16,40}, F. Fontanelli^{20,h},
 R. Forty⁴⁰, V. Franco Lima⁵⁴, M. Frank⁴⁰, C. Frei⁴⁰, J. Fu^{22,q},
 W. Funk⁴⁰, E. Furfaro^{25,j}, C. Färber⁴⁰, E. Gabriel⁵², A. Gallas Torreira³⁹,
 D. Galli^{15,e}, S. Gallorini²³, S. Gambetta⁵², M. Gandelman², P. Gandini²²,
 Y. Gao³, L.M. Garcia Martin⁷⁰, J. García Pardiñas³⁹, J. Garra Tico⁴⁹,
 L. Garrido³⁸, D. Gascon³⁸, C. Gaspar⁴⁰, L. Gavardi¹⁰, G. Gazzoni⁵,

D. Gerick¹², E. Gersabeck⁵⁶, M. Gersabeck⁵⁶, T. Gershon⁵⁰, Ph. Ghez⁴,
 S. Gianì⁴¹, V. Gibson⁴⁹, O.G. Girard⁴¹, L. Giubega³⁰, K. Gizdov⁵²,
 V.V. Gligorov⁸, D. Golubkov³², A. Golutvin⁵⁵, A. Gomes^{1,a},
 I.V. Gorelov³³, C. Gotti^{21,i}, E. Govorkova⁴³, J.P. Grabowski¹²,
 R. Graciani Diaz³⁸, L.A. Granado Cardoso⁴⁰, E. Graugés³⁸,
 E. Graverini⁴², G. Graziani¹⁸, A. Greco³⁰, R. Greim⁹, P. Griffith¹⁶,
 L. Grillo⁵⁶, L. Gruber⁴⁰, B.R. Gruberg Cazon⁵⁷, O. Grünberg⁶⁷,
 E. Gushchin³⁴, Yu. Guz³⁷, T. Gys⁴⁰, C. Göbel⁶², T. Hadavizadeh⁵⁷,
 C. Hadjivasiliou⁵, G. Haefeli⁴¹, C. Haen⁴⁰, S.C. Haines⁴⁹,
 B. Hamilton⁶⁰, X. Han¹², T.H. Hancock⁵⁷, S. Hansmann-Menzemer¹²,
 N. Harnew⁵⁷, S.T. Harnew⁴⁸, C. Hasse⁴⁰, M. Hatch⁴⁰, J. He⁶³,
 M. Hecker⁵⁵, K. Heinicke¹⁰, A. Heister⁹, K. Hennessy⁵⁴, P. Henrard⁵,
 L. Henry⁷⁰, E. van Herwijnen⁴⁰, M. Heß⁶⁷, A. Hicheur², D. Hill⁵⁷,
 P.H. Hopchev⁴¹, W. Hu⁶⁵, W. Huang⁶³, Z.C. Huard⁵⁹, W. Hulsbergen⁴³,
 T. Humair⁵⁵, M. Hushchyn³⁵, D. Hutchcroft⁵⁴, P. Ibis¹⁰, M. Idzik²⁸,
 P. Ilten⁴⁷, R. Jacobsson⁴⁰, J. Jalocha⁵⁷, E. Jans⁴³, A. Jawahery⁶⁰,
 F. Jiang³, M. John⁵⁷, D. Johnson⁴⁰, C.R. Jones⁴⁹, C. Joram⁴⁰, B. Jost⁴⁰,
 N. Jurik⁵⁷, S. Kandybei⁴⁵, M. Karacson⁴⁰, J.M. Kariuki⁴⁸, S. Karodia⁵³,
 N. Kazeev³⁵, M. Kecke¹², F. Keizer⁴⁹, M. Kelsey⁶¹, M. Kenzie⁴⁹,
 T. Ketel⁴⁴, E. Khairullin³⁵, B. Khanji¹², C. Khurewathanakul⁴¹, T. Kirn⁹,
 S. Klaver¹⁹, K. Klimaszewski²⁹, T. Klimovich¹¹, S. Koliiev⁴⁶,
 M. Kolpin¹², R. Kopečna¹², P. Koppenburg⁴³, A. Kosmyntseva³²,
 S. Kotriakhova³¹, M. Kozeiha⁵, L. Kravchuk³⁴, M. Kreps⁵⁰, F. Kress⁵⁵,
 P. Krokovny^{36,w}, W. Krzemien²⁹, W. Kucewicz^{27,l}, M. Kucharczyk²⁷,
 V. Kudryavtsev^{36,w}, A.K. Kuonen⁴¹, T. Kvaratskheliya^{32,40},
 D. Lacarrere⁴⁰, G. Lafferty⁵⁶, A. Lai¹⁶, G. Lanfranchi¹⁹,
 C. Langenbruch⁹, T. Latham⁵⁰, C. Lazzeroni⁴⁷, R. Le Gac⁶,
 A. Leflat^{33,40}, J. Lefrançois⁷, R. Lefèvre⁵, F. Lemaitre⁴⁰,
 E. Lemos Cid³⁹, O. Leroy⁶, T. Lesiak²⁷, B. Leverington¹², P.-R. Li⁶³,
 T. Li³, Y. Li⁷, Z. Li⁶¹, X. Liang⁶¹, T. Likhomanenko⁶⁸, R. Lindner⁴⁰,
 F. Lionetto⁴², V. Lisovskyi⁷, X. Liu³, D. Loh⁵⁰, A. Loi¹⁶, I. Longstaff⁵³,
 J.H. Lopes², D. Lucchesi^{23,o}, M. Lucio Martinez³⁹, H. Luo⁵²,
 A. Lupato²³, E. Luppi^{17,g}, O. Lupton⁴⁰, A. Lusiani²⁴, X. Lyu⁶³,
 F. Machefert⁷, F. Maciuc³⁰, V. Macko⁴¹, P. Mackowiak¹⁰,
 S. Maddrell-Mander⁴⁸, O. Maev^{31,40}, K. Maguire⁵⁶, D. Maisuzenko³¹,
 M.W. Majewski²⁸, S. Malde⁵⁷, B. Malecki²⁷, A. Malinin⁶⁸,
 T. Maltsev^{36,w}, G. Manca^{16,f}, G. Mancinelli⁶, D. Marangotto^{22,q},

J. Maratas^{5,v}, J.F. Marchand⁴, U. Marconi¹⁵, C. Marin Benito³⁸,
 M. Marinangeli⁴¹, P. Marino⁴¹, J. Marks¹², G. Martellotti²⁶, M. Martin⁶,
 M. Martinelli⁴¹, D. Martinez Santos³⁹, F. Martinez Vidal⁷⁰,
 A. Massafferri¹, R. Matev⁴⁰, A. Mathad⁵⁰, Z. Mathe⁴⁰, C. Matteuzzi²¹,
 A. Mauri⁴², E. Maurice^{7,b}, B. Maurin⁴¹, A. Mazurov⁴⁷, M. McCann^{55,40},
 A. McNab⁵⁶, R. McNulty¹³, J.V. Mead⁵⁴, B. Meadows⁵⁹, C. Meaux⁶,
 F. Meier¹⁰, N. Meinert⁶⁷, D. Melnychuk²⁹, M. Merk⁴³, A. Merli^{22,40,q},
 E. Michielin²³, D.A. Milanes⁶⁶, E. Millard⁵⁰, M.-N. Minard⁴,
 L. Minzoni¹⁷, D.S. Mitzel¹², A. Mogini⁸, J. Molina Rodriguez¹,
 T. Mombächer¹⁰, I.A. Monroy⁶⁶, S. Monteil⁵, M. Morandin²³,
 M.J. Morello^{24,t}, O. Morgunova⁶⁸, J. Moron²⁸, A.B. Morris⁵²,
 R. Mountain⁶¹, F. Muheim⁵², M. Mulder⁴³, D. Müller⁵⁶, J. Müller¹⁰,
 K. Müller⁴², V. Müller¹⁰, P. Naik⁴⁸, T. Nakada⁴¹, R. Nandakumar⁵¹,
 A. Nandi⁵⁷, I. Nasteva², M. Needham⁵², N. Neri^{22,40}, S. Neubert¹²,
 N. Neufeld⁴⁰, M. Neuner¹², T.D. Nguyen⁴¹, C. Nguyen-Mau^{41,n},
 S. Nieswand⁹, R. Niet¹⁰, N. Nikitin³³, T. Nikodem¹², A. Nogay⁶⁸,
 D.P. O’Hanlon⁵⁰, A. Oblakowska-Mucha²⁸, V. Obraztsov³⁷, S. Ogilvy¹⁹,
 R. Oldeman^{16,f}, C.J.G. Onderwater⁷¹, A. Ossowska²⁷,
 J.M. Otalora Goicochea², P. Owen⁴², A. Oyanguren⁷⁰, P.R. Pais⁴¹,
 A. Palano¹⁴, M. Palutan^{19,40}, A. Papanestis⁵¹, M. Pappagallo⁵²,
 L.L. Pappalardo^{17,g}, W. Parker⁶⁰, C. Parkes⁵⁶, G. Passaleva^{18,40},
 A. Pastore^{14,d}, M. Patel⁵⁵, C. Patrignani^{15,e}, A. Pearce⁴⁰, A. Pellegrino⁴³,
 G. Penso²⁶, M. Pepe Altarelli⁴⁰, S. Perazzini⁴⁰, D. Pereima³², P. Perret⁵,
 L. Pescatore⁴¹, K. Petridis⁴⁸, A. Petrolini^{20,h}, A. Petrov⁶⁸,
 M. Petruzzo^{22,q}, E. Picatoste Olloqui³⁸, B. Pietrzyk⁴, G. Pietrzyk⁴¹,
 M. Pikies²⁷, D. Pinci²⁶, F. Pisani⁴⁰, A. Pistone^{20,h}, A. Piucci¹²,
 V. Placinta³⁰, S. Playfer⁵², M. Plo Casasus³⁹, F. Polci⁸, M. Poli Lener¹⁹,
 A. Poluektov⁵⁰, I. Polyakov⁶¹, E. Polycarpo², G.J. Pomery⁴⁸, S. Ponce⁴⁰,
 A. Popov³⁷, D. Popov^{11,40}, S. Poslavskii³⁷, C. Potterat², E. Price⁴⁸,
 J. Prisciandaro³⁹, C. Prouve⁴⁸, V. Pugatch⁴⁶, A. Puig Navarro⁴²,
 H. Pullen⁵⁷, G. Punzi^{24,p}, W. Qian⁵⁰, J. Qin⁶³, R. Quagliani⁸,
 B. Quintana⁵, B. Rachwal²⁸, J.H. Rademacker⁴⁸, M. Rama²⁴,
 M. Ramos Pernas³⁹, M.S. Rangel², I. Raniuk^{45,†}, F. Ratnikov³⁵,
 G. Raven⁴⁴, M. Ravonel Salzgeber⁴⁰, M. Reboud⁴, F. Redi⁴¹,
 S. Reichert¹⁰, A.C. dos Reis¹, C. Remon Alepuz⁷⁰, V. Renaudin⁷,
 S. Ricciardi⁵¹, S. Richards⁴⁸, M. Rihl⁴⁰, K. Rinnert⁵⁴, P. Robbe⁷,
 A. Robert⁸, A.B. Rodrigues⁴¹, E. Rodrigues⁵⁹, J.A. Rodriguez Lopez⁶⁶,

A. Rogozhnikov³⁵, S. Roiser⁴⁰, A. Rollings⁵⁷, V. Romanovskiy³⁷,
 A. Romero Vidal^{39,40}, M. Rotondo¹⁹, M.S. Rudolph⁶¹, T. Ruf⁴⁰,
 P. Ruiz Valls⁷⁰, J. Ruiz Vidal⁷⁰, J.J. Saborido Silva³⁹, E. Sadykhov³²,
 N. Sagidova³¹, B. Saitta^{16,f}, V. Salustino Guimaraes⁶²,
 C. Sanchez Mayordomo⁷⁰, B. Sanmartin Sedes³⁹, R. Santacesaria²⁶,
 C. Santamarina Rios³⁹, M. Santimaria¹⁹, E. Santovetti^{25,j}, G. Sarpis⁵⁶,
 A. Sarti^{19,k}, C. Satriano^{26,s}, A. Satta²⁵, D.M. Saunders⁴⁸, D. Savrina^{32,33},
 S. Schael⁹, M. Schellenberg¹⁰, M. Schiller⁵³, H. Schindler⁴⁰,
 M. Schmelling¹¹, T. Schmelzer¹⁰, B. Schmidt⁴⁰, O. Schneider⁴¹,
 A. Schopper⁴⁰, H.F. Schreiner⁵⁹, M. Schubiger⁴¹, M.H. Schune⁷,
 R. Schwemmer⁴⁰, B. Sciascia¹⁹, A. Sciubba^{26,k}, A. Semennikov³²,
 E.S. Sepulveda⁸, A. Sergi⁴⁷, N. Serra⁴², J. Serrano⁶, L. Sestini²³,
 P. Seyfert⁴⁰, M. Shapkin³⁷, I. Shapoval⁴⁵, Y. Shcheglov³¹, T. Shears⁵⁴,
 L. Shekhtman^{36,w}, V. Shevchenko⁶⁸, B.G. Siddi¹⁷, R. Silva Coutinho⁴²,
 L. Silva de Oliveira², G. Simi^{23,o}, S. Simone^{14,d}, M. Sirendi⁴⁹,
 N. Skidmore⁴⁸, T. Skwarnicki⁶¹, I.T. Smith⁵², J. Smith⁴⁹, M. Smith⁵⁵,
 I. Soares Lavra¹, M.D. Sokoloff⁵⁹, F.J.P. Soler⁵³, B. Souza De Paula²,
 B. Spaan¹⁰, P. Spradlin⁵³, S. Sridharan⁴⁰, F. Stagni⁴⁰, M. Stahl¹²,
 S. Stahl⁴⁰, P. Stefko⁴¹, S. Stefkova⁵⁵, O. Steinkamp⁴², S. Stemmler¹²,
 O. Stenyakin³⁷, M. Stepanova³¹, H. Stevens¹⁰, S. Stone⁶¹, B. Storaci⁴²,
 S. Stracka^{24,p}, M.E. Stramaglia⁴¹, M. Straticiuc³⁰, U. Straumann⁴²,
 J. Sun³, L. Sun⁶⁴, K. Swientek²⁸, V. Syropoulos⁴⁴, T. Szumlak²⁸,
 M. Szymanski⁶³, S. T’Jampens⁴, A. Tayduganov⁶, T. Tekampe¹⁰,
 G. Tellarini^{17,g}, F. Teubert⁴⁰, E. Thomas⁴⁰, J. van Tilburg⁴³,
 M.J. Tilley⁵⁵, V. Tisserand⁵, M. Tobin⁴¹, S. Tolk⁴⁹, L. Tomassetti^{17,g},
 D. Tonelli²⁴, R. Tourinho Jadallah Aoude¹, E. Tournefier⁴, M. Traill⁵³,
 M.T. Tran⁴¹, M. Tresch⁴², A. Trisovic⁴⁹, A. Tsaregorodtsev⁶,
 P. Tsopelas⁴³, A. Tully^{49,*}, N. Tuning^{43,40}, A. Ukleja²⁹, A. Usachov⁷,
 A. Ustyuzhanin³⁵, U. Uwer¹², C. Vacca^{16,f}, A. Vagner⁶⁹, V. Vagnoni^{15,40},
 A. Valassi⁴⁰, S. Valat⁴⁰, G. Valenti¹⁵, R. Vazquez Gomez⁴⁰,
 P. Vazquez Regueiro³⁹, S. Vecchi¹⁷, M. van Veghel⁴³, J.J. Velthuis⁴⁸,
 M. Veltri^{18,r}, G. Veneziano⁵⁷, A. Venkateswaran⁶¹, T.A. Verlage⁹,
 M. Vernet⁵, M. Vesterinen⁵⁷, J.V. Viana Barbosa⁴⁰, D. Vieira⁶³,
 M. Vieites Diaz³⁹, H. Viemann⁶⁷, X. Vilasis-Cardona^{38,m}, M. Vitti⁴⁹,
 V. Volkov³³, A. Vollhardt⁴², B. Voneki⁴⁰, A. Vorobyev³¹,
 V. Vorobyev^{36,w}, C. Voß⁹, J.A. de Vries⁴³, C. Vázquez Sierra⁴³,
 R. Waldi⁶⁷, J. Walsh²⁴, J. Wang⁶¹, Y. Wang⁶⁵, D.R. Ward⁴⁹,

H.M. Wark⁵⁴, N.K. Watson⁴⁷, D. Websdale⁵⁵, A. Weiden⁴²,
 C. Weisser⁵⁸, M. Whitehead⁴⁰, J. Wicht⁵⁰, G. Wilkinson⁵⁷,
 M. Wilkinson⁶¹, M. Williams⁵⁶, M. Williams⁵⁸, T. Williams⁴⁷,
 F.F. Wilson^{51,40}, J. Wimberley⁶⁰, M. Winn⁷, J. Wishahi¹⁰, W. Wislicki²⁹,
 M. Witek²⁷, G. Wormser⁷, S.A. Wotton⁴⁹, K. Wyllie⁴⁰, Y. Xie⁶⁵,
 M. Xu⁶⁵, Q. Xu⁶³, Z. Xu³, Z. Xu⁴, Z. Yang³, Z. Yang⁶⁰, Y. Yao⁶¹,
 H. Yin⁶⁵, J. Yu⁶⁵, X. Yuan⁶¹, O. Yushchenko³⁷, K.A. Zarebski⁴⁷,
 M. Zavertyaev^{11,c}, L. Zhang³, Y. Zhang⁷, A. Zhelezov¹², Y. Zheng⁶³,
 X. Zhu³, V. Zhukov^{9,33}, J.B. Zonneveld⁵², S. Zucchelli¹⁵

¹ Centro Brasileiro de Pesquisas Físicas (CBPF), Rio de Janeiro, Brazil

² Universidade Federal do Rio de Janeiro (UFRJ), Rio de Janeiro, Brazil

³ Center for High Energy Physics, Tsinghua University, Beijing, China

⁴ Univ. Grenoble Alpes, Univ. Savoie Mont Blanc, CNRS, IN2P3-LAPP, Annecy, France

⁵ Clermont Université, Université Blaise Pascal, CNRS/IN2P3, LPC, Clermont-Ferrand, France

⁶ Aix Marseille Univ, CNRS/IN2P3, CPPM, Marseille, France

⁷ LAL, Univ. Paris-Sud, CNRS/IN2P3, Université Paris-Saclay, Orsay, France

⁸ LPNHE, Université Pierre et Marie Curie, Université Paris Diderot, CNRS/IN2P3, Paris, France

⁹ I. Physikalisches Institut, RWTH Aachen University, Aachen, Germany

¹⁰ Fakultät Physik, Technische Universität Dortmund, Dortmund, Germany

¹¹ Max-Planck-Institut für Kernphysik (MPIK), Heidelberg, Germany

¹² Physikalisches Institut, Ruprecht-Karls-Universität Heidelberg, Heidelberg, Germany

¹³ School of Physics, University College Dublin, Dublin, Ireland

¹⁴ Sezione INFN di Bari, Bari, Italy

¹⁵ Sezione INFN di Bologna, Bologna, Italy

¹⁶ Sezione INFN di Cagliari, Cagliari, Italy

¹⁷ Università e INFN, Ferrara, Ferrara, Italy

¹⁸ Sezione INFN di Firenze, Firenze, Italy

¹⁹ Laboratori Nazionali dell'INFN di Frascati, Frascati, Italy

²⁰ Sezione INFN di Genova, Genova, Italy

²¹ Sezione INFN di Milano Bicocca, Milano, Italy

²² Sezione di Milano, Milano, Italy

²³ Sezione INFN di Padova, Padova, Italy

²⁴ Sezione INFN di Pisa, Pisa, Italy

²⁵ Sezione INFN di Roma Tor Vergata, Roma, Italy

²⁶ Sezione INFN di Roma La Sapienza, Roma, Italy

²⁷ Henryk Niewodniczanski Institute of Nuclear Physics Polish Academy of Sciences, Kraków, Poland

²⁸ AGH – University of Science and Technology, Faculty of Physics and Applied Computer Science, Kraków, Poland

²⁹ National Center for Nuclear Research (NCBJ), Warsaw, Poland

³⁰ Horia Hulubei National Institute of Physics and Nuclear Engineering, Bucharest-Magurele, Romania

³¹ Petersburg Nuclear Physics Institute (PNPI), Gatchina, Russia

³² Institute of Theoretical and Experimental Physics (ITEP), Moscow, Russia

³³ Institute of Nuclear Physics, Moscow State University (SINP MSU), Moscow, Russia

³⁴ Institute for Nuclear Research of the Russian Academy of Sciences (INR RAN), Moscow, Russia

³⁵ Yandex School of Data Analysis, Moscow, Russia

³⁶ Budker Institute of Nuclear Physics (SB RAS), Novosibirsk, Russia

³⁷ Institute for High Energy Physics (IHEP), Protvino, Russia

³⁸ ICCUB, Universitat de Barcelona, Barcelona, Spain

³⁹ Instituto Galego de Física de Altas Enerxías (IGFAE), Universidade de Santiago de Compostela, Santiago de Compostela, Spain

⁴⁰ European Organization for Nuclear Research (CERN), Geneva, Switzerland

⁴¹ Institute of Physics, Ecole Polytechnique Fédérale de Lausanne (EPFL), Lausanne, Switzerland

- ⁴² Physik-Institut, Universität Zürich, Zürich, Switzerland
- ⁴³ Nikhef National Institute for Subatomic Physics, Amsterdam, the Netherlands
- ⁴⁴ Nikhef National Institute for Subatomic Physics and VU University Amsterdam, Amsterdam, the Netherlands
- ⁴⁵ NSC Kharkiv Institute of Physics and Technology (NSC KIPT), Kharkiv, Ukraine
- ⁴⁶ Institute for Nuclear Research of the National Academy of Sciences (KINR), Kyiv, Ukraine
- ⁴⁷ University of Birmingham, Birmingham, United Kingdom
- ⁴⁸ H.H. Wills Physics Laboratory, University of Bristol, Bristol, United Kingdom
- ⁴⁹ Cavendish Laboratory, University of Cambridge, Cambridge, United Kingdom
- ⁵⁰ Department of Physics, University of Warwick, Coventry, United Kingdom
- ⁵¹ STFC Rutherford Appleton Laboratory, Didcot, United Kingdom
- ⁵² School of Physics and Astronomy, University of Edinburgh, Edinburgh, United Kingdom
- ⁵³ School of Physics and Astronomy, University of Glasgow, Glasgow, United Kingdom
- ⁵⁴ Oliver Lodge Laboratory, University of Liverpool, Liverpool, United Kingdom
- ⁵⁵ Imperial College London, London, United Kingdom
- ⁵⁶ School of Physics and Astronomy, University of Manchester, Manchester, United Kingdom
- ⁵⁷ Department of Physics, University of Oxford, Oxford, United Kingdom
- ⁵⁸ Massachusetts Institute of Technology, Cambridge, MA, United States
- ⁵⁹ University of Cincinnati, Cincinnati, OH, United States
- ⁶⁰ University of Maryland, College Park, MD, United States
- ⁶¹ Syracuse University, Syracuse, NY, United States
- ⁶² Pontifícia Universidade Católica do Rio de Janeiro (PUC-Rio), Rio de Janeiro, Brazil, associated to ²
- ⁶³ University of Chinese Academy of Sciences, Beijing, China, associated to ³
- ⁶⁴ School of Physics and Technology, Wuhan University, Wuhan, China, associated to ³
- ⁶⁵ Institute of Particle Physics, Central China Normal University, Wuhan, Hubei, China, associated to ³
- ⁶⁶ Departamento de Física, Universidad Nacional de Colombia, Bogotá, Colombia, associated to ⁸
- ⁶⁷ Institut für Physik, Universität Rostock, Rostock, Germany, associated to ¹²
- ⁶⁸ National Research Centre Kurchatov Institute, Moscow, Russia, associated to ³²
- ⁶⁹ National Research Tomsk Polytechnic University, Tomsk, Russia, associated to ³²
- ⁷⁰ Instituto de Física Corpuscular, Centro Mixto Universidad de Valencia – CSIC, Valencia, Spain, associated to ³⁸
- ⁷¹ Van Swinderen Institute, University of Groningen, Groningen, the Netherlands, associated to ⁴³
- ⁷² Los Alamos National Laboratory (LANL), Los Alamos, United States, associated to ⁶¹

* Corresponding author.

E-mail address: alison.tully@cern.ch (A. Tully).

- ^a Universidade Federal do Triângulo Mineiro (UFTM), Uberaba, MG, Brazil.
- ^b Laboratoire Leprince-Ringuet, Palaiseau, France.
- ^c P.N. Lebedev Physical Institute, Russian Academy of Science (LPI RAS), Moscow, Russia.
- ^d Università di Bari, Bari, Italy.
- ^e Università di Bologna, Bologna, Italy.
- ^f Università di Cagliari, Cagliari, Italy.
- ^g Università di Ferrara, Ferrara, Italy.
- ^h Università di Genova, Genova, Italy.
- ⁱ Università di Milano Bicocca, Milano, Italy.
- ^j Università di Roma Tor Vergata, Roma, Italy.
- ^k Università di Roma La Sapienza, Roma, Italy.
- ^l AGH – University of Science and Technology, Faculty of Computer Science, Electronics and Telecommunications, Kraków, Poland.
- ^m LIFAELS, La Salle, Universitat Ramon Llull, Barcelona, Spain.
- ⁿ Hanoi University of Science, Hanoi, Viet Nam.
- ^o Università di Padova, Padova, Italy.
- ^p Università di Pisa, Pisa, Italy.
- ^q Università degli Studi di Milano, Milano, Italy.
- ^r Università di Urbino, Urbino, Italy.
- ^s Università della Basilicata, Potenza, Italy.

^t Scuola Normale Superiore, Pisa, Italy.

^u Università di Modena e Reggio Emilia, Modena, Italy.

^v Iligan Institute of Technology (IIT), Iligan, Philippines.

^w Novosibirsk State University, Novosibirsk, Russia.

[†] Deceased.